Additive Manufacturing 28 (2019) 629–638

Contents lists available at ScienceDirect

Additive Manufacturing

journal homepage: www.elsevier.com/locate/addma

Multi-material 3D printing of a soft pressure sensor

Md Omar Faruk Emon[a], Faez Alkadi[a,d], Daryl George Philip[a], Da-Hye Kim[b], Kyung-Chang Lee[c], Jae-Won Choi[a,c,*]

[a] Department of Mechanical Engineering, The University of Akron, 244 Sumner Street, Akron, OH, 44325-3903, United States
[b] Extreme Fabrication Technology Group, Korea Institute of Industrial Technology, Daegu, 42994, Republic of Korea
[c] Department of Control and Instrumentation Engineering, Pukyong National University, Busan 48513, Republic of Korea
[d] The Department of Mechanical Engineering, Jazan University, Jazan 45142, Saudi Arabia

ARTICLE INFO

Keywords:
3D printing
Stretchable electronics
Ionic liquid
Soft pressure sensor
Multi-Material direct-print

ABSTRACT

The emergence of smart technologies is spurring the development of a wider range of applications for stretchable and conformable sensors, as the design flexibility offered by additive manufacturing may enable the production of sensors that are superior to those produced by conventional manufacturing techniques. In this work, a multi-material 3D printing system with three extrusion heads was developed to fabricate a stretchable, soft pressure sensor built using an ionic liquid (IL)–based pressure-sensitive layer that was sandwiched between carbon nanotube (CNT)–based stretchable electrodes and encapsulated within stretchable top and bottom insulating layers. The sensor materials were modified in order to achieve 3D printable characteristics. The capability of the system was tested by printing structures made from three materials and a multilayer sensor via an extrusion-based direct-print process. Multi-material 3D printing of the sensor was successfully realized, as the sensing material retained its functionality once the printing process was complete.

1. Introduction

Smart technologies are now on the rise, and many smart devices require flexibility and stretchability [1–3]. Robotics [4], prosthetics [5,6], wearable electronics [7,8], and energy harvesting devices [9] are examples of technologies where soft and stretchable electronics would play an important role. In particular, flexible and stretchable sensors are gaining more attention because of their applications in shape-conforming systems or systems that have moveable parts [10,11]. One major area of such applications is wearable electronics for recreational use [12], medical/healthcare devices [13], and personal protection [14,15]. Along with mechanical flexibility, wearable devices that are in contact with the human body must also be designed to minimize discomfort and absorb some impact [16]. In addition to wearable devices, stretchable sensors might be used in other soft smart systems whose concepts are being explored such as tires [17], mattresses [18], packaging [19], automobile accessories [20], and non-wearable medical devices [21]. In many cases, rigid sensors are incompatible with deformable and free-form objects, generating the interest for sensors that are mechanically pliable.

Numerous studies on flexible and stretchable sensors have been conducted in the past decade. One common strategy to achieve stretchability in sensors is to use a stretchable polymer with conductive fillers. Carbon nanotube (CNT)–based piezoresistive sensors are among the more widely studied ones [22,23]; however, their reliability and controllability are limited [24,25]. The recent introduction of ionic liquids (ILs) to the area of pressure sensors opened a new avenue of exploration for stretchable sensors [26,27]. ILs, which are composed of liquid salt at ambient temperature and contain ions, have highly sought-after characteristics such as high ionic conductivity, non-volatility, nonflammability, and most importantly electrochemical stability [28,29]. While ILs have been utilized to fabricate various devices for sensing, those that are in a liquid state have very limited application [30,31]. Some studies have been published on solid-state IL-based sensors, but they generally lack manufacturing and design flexibility [27,32]. In a prior work, the authors incorporated ILs into a prepolymer matrix to fabricate a solid-state pressure-sensitive film through polymerization [26,33] to obtain an IL/polymer network with high electrical resistance that changes under mechanical strain. This system was utilized as the sensing principle in the pressure sensor. A CNT/polymer composite was used as the conductive electrode for fabricating the stretchable pressure sensor. Incorporating ILs into the pressure sensor provides more control over the sensing performance.

Along with research on functional materials, the fabrication process

* Corresponding author at: Department of Mechanical Engineering, The University of Akron, 244 Sumner Street, Akron, OH, 44325-3903, United States.
E-mail address: jchoi1@uakron.edu (J.-W. Choi).

https://doi.org/10.1016/j.addma.2019.06.001
Received 6 May 2019; Received in revised form 3 June 2019; Accepted 4 June 2019
Available online 04 June 2019
2214-8604/

for soft sensors has garnered more attention in recent years. The various manufacturing techniques that have been suggested for fabricating soft sensors include injection molding [34], coating [35], the fill and lamination process [36], and screen printing [37]. Although these methods are appropriate for building sensors with simple geometries, they are unsuitable for fabricating sensors with complex geometries or for sensors on free-form surfaces. 3D printing overcomes the limitations of conventional manufacturing processes, offering design flexibility, customizability, and manufacturing scalability [38,39]. In many cases, especially those where sensors are not required to be mass-produced, 3D printing reduces costs, as the printing of different designs does not involve changing the manufacturing setup for each product. In addition, 3D printing is preferred over traditional methods for the manufacturing of objects/parts that contain internal features or that need to be built using multiple materials. Moreover, for an application that employs tactile sensors on human-machine interfaces and for prosthetics or robotics, free-form surfaces are involved; 3D printing could be a possible solution for fabricating electronics on a free-form, non-flat substrate [40].

Different 3D printing technologies, such as thermoplastic extrusion [41], stereolithography [42], material or binder jetting [43], and powder bed fusion [44] support fabrication using a broad selection of materials. Recent developments in additive manufacturing have enabled the 3D printing of soft electronics with functional materials [45]. Extrusion-based direct-print (also referred to as *direct write*) is a suitable technique to use for 3D printing functional materials [46,47]. Thermosetting prepolymers are commonly functionalized and modified for printing in cases where heat or light are used for subsequent polymerization, and viscoelastic elastomers could be used for printing in cases where there is a need to build flexible and stretchable parts. Despite the work conducted in the area of 3D printing of functional materials, there is still a need for additional work in order to achieve a printing process that uses multiple materials in a single print, to facilitate the introduction of ILs for functionalizing, and to optimize soft/stretchable polymers for printing.

In this study, we developed a multi-material direct-print system to 3D print a soft pressure sensor. A prepolymer paste was used in the system for a layer-by-layer extrusion-based printing. Next, the 3D printed prepolymer part was polymerized through a combination of photo and thermal curing processes. The multi-layer sensor incorporates three different materials for the insulation, the conductive electrodes, and the pressure-sensitive layer. For the pressure-sensitive layer, ILs were mixed with a prepolymer to induce pressure sensitivity. The inclusion of IL into the sensor gives more flexibility in controlling sensor performance. By varying the IL ratio, the sensitivity of the sensor can be adjusted to achieve different dynamic ranges. The sensor design and geometry can also be varied to modulate the sensing performance. The multi-material direct-print system provides a solution to tailor material compositions and geometry for the development of a subject/application-specific sensor.

2. Materials and method

2.1. Sensor design

The proposed sensor is a multi-layer IL-based pressure sensor with five stretchable layers, as shown in Fig. 1. The top and bottom layers are insulation layers fabricated using a soft polymer. The innermost layer is an intermediate pressure-sensitive layer that is based on a soft IL/polymer network film. Between the intermediate layer and the top and bottom insulating layers are electrodes that are based on a multi-walled carbon nanotube (MWCNT)/polymer composite and act as stretchable conductive wires. A sensing unit called a *taxel* (i.e., tactile pixel) is created at each point where the electrodes cross, as indicated by the areas circled in red in Fig. 1(a). The particular sensor shown in this figure contains four taxels in a 2 × 2 electrode configuration, but other sensing array configurations having a different number of taxels can be designed by varying the number of electrodes that are sandwiched between the pressure-sensitive layer and the two insulation layers.

The incorporation of ILs into the intermediate layer of the sensor enhances ionic conductivity. An external power supply is used to create a potential difference between the electrodes of a taxel, which is the pressure-sensitive zone in the sensor. When a compressive force is applied on the taxel, the electrical resistance of the intermediate layer decreases due to deformation. As the output voltage from the sensor system depends on the resistance of the taxel, the response of the sensor under force is measured in terms of output voltage.

Since it is possible for a MWCNT-based electrode to have a piezoresistive effect, which is not desirable for the proposed sensor, the intermediate layer was designed such that its resistance would be much higher than that of the electrode, compelling the intermediate layer to become the dominant factor under force. In order to realize this condition, a high loading ratio of MWCNT (5 wt.%) is used in the fabrication of the electrode material, which is a higher than the electrical percolation threshold of the MWCNT/polymer composites [48]. Thus, the IL-based intermediate layer will define and govern the sensing performance.

2.2. Materials

The base material used to fabricate the sensor is the photopolymer TangoPlus FLX930 (Stratasys, Eden Prairie, Minn., USA), which has been utilized in commercial multi-jet 3D printers. Once TangoPlus is polymerized through the use of ultra-violet (UV) light, it creates a flexible and stretchable film. However, for the extrusion-based direct-print system proposed in this study, TangoPlus was modified in order to obtain the desired shear thinning property. Fig. 2 shows TangoPlus before and after modification with 10 wt.% CAB-O-SIL® M5 fumed silica (Cabot Corporation, Billerica, Mass., USA) that has a higher viscosity [49]. To achieve the modification, fumed silica was mixed with TangoPlus using a DAC 150.1 FVZ-K high-speed mixer (FlackTek, Inc., Landrum, S.C., USA) at 2500 rpm for five minutes. Fig. 2(c) demonstrates the extrusion of modified TangoPlus through the printing nozzle, where the modified prepolymer has a shear thinning property that enables it to hold the filament shape following extrusion. The modified TangoPlus was used for both the top and bottom insulation layers of the sensor. For the pressure-sensitive intermediate layer, an ionic liquid, 1-ethyl-3-methylimidazolium tetrafluoroborate (EMIBF4; obtained from Sigma-Aldrich) was mixed with TangoPlus in the high-speed mixer, where IL ratio was 4 wt.% [50]. Again, in order to achieve the proper viscosity and shear thinning, 10 wt.% fumed silica was added to the IL/prepolymer blend.

The conductive electrode material was prepared by dispersing 5 wt.% MWCNTs (having a length of 5–20 μm, a diameter of 10–30 nm, and a purity greater than 85%) into TangoPlus. This was accomplished by first dissolving Triton X100 surfactant (Sigma-Aldrich, Milwaukee, Wisc., USA) into dimethylformamide (DMF; Sigma-Aldrich) before adding MWCNTs to the solution; a ratio of 1.0:3.5 MWCNTs to Triton X100 was used. The solution was sonicated using a Qsonica Q700 sonicator (Newtown, Ct., USA) to obtain global dispersion. Following sonication, TangoPlus was added to the DMF/MWCNT solution, which was mixed using a VWR 10 × 10-in. (25.4 × 25.4-cm) aluminum hot plate magnetic stirrer (VWR, Chicago, Ill., USA). After evaporation of the solvent, the paste was mixed again using a high-speed mixer at 2500 rpm. In order to induce the material to become thermally curable, 2 wt.% of a thermal initiator (Trigonox 125-C75, AkzoNobel Functional Chemicals LLC, Chicago, Ill., USA) was added to the paste to facilitate screen printing of the MWCNT/prepolymer electrode [50]; however, when used for 3D printing/direct-print, the use of this paste resulted in inconsistent printing. The addition of fumed silica to the paste improved its performance for 3D printing. As can be noticed from Fig. 3(a), using a CNT/prepolymer without fumed silica for 3D printing

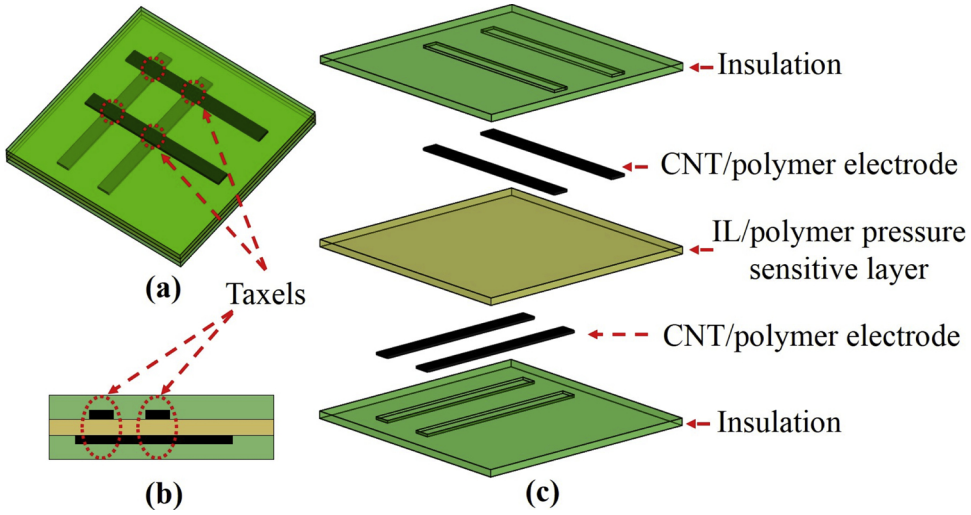

Fig. 1. Design for a 4-taxel sensor: (*a*) 3D model of the sensor; (*b*) schematic diagram showing a side view of the sensor; (*c*) exploded view of the sensor showing the individual layers.

results in inconsistent line widths and printed lines that are unable to retain their shape.

Although the addition of fumed silica improved the printability of the electrode, it degraded the electrical conductivity of the CNT/polymer electrode material. To investigate the effect of fumed silica on electrical conductivity, CNT/polymer lines (1 mm × 40 mm) were screen-printed with different wt.% of fumed silica. From Fig. 3(c), it can be noticed that the incorporation of fumed silica increased the resistance of the CNT/polymer line, which is an undesirable outcome. Moreover, beyond 8 wt.% of fumed silica, the printed CNT/polymer line was noticed to crack upon curing. The use of 4–5 wt.% fumed silica in the CNT/polymer yielded a material with reasonable conductivity that was able to produce a consistent print, as shown in Fig. 3(b). Thus, 5 wt.% fumed silica was added to the CNT/prepolymer composite used for printing the electrodes in the stretchable sensor developed in this study.

2.3. Multi-material direct-print

A multi-material extrusion-based direct-print system was developed to 3D print the soft pressure sensor. Since the sensor is composed of three different materials, a printing system was developed with three extrusion heads capable of printing three different materials in a single print. A high- precision motorized XYZ linear stage system (PRO115, Aerotech Inc., Pittsburgh, Pa., USA) was used for the movement of the axis, as shown in Fig. 4. Three extruders/syringes with three XR25C/M manual translation stages (Thorlabs Inc., Newton, N.*J*., USA) were installed on the Z-stage to enable fine adjustment during the extruder calibration. Each extruder was connected to an air-based Ultimus I pressure controller (Nordson EFD, East Providence, R.I., USA); the pressure controllers were interfaced with *LabVIEW*, where the stage movement and material dispensing processes were coordinated using G-code instructions in the Aerotech software environment. Extrusion nozzles with sizes ranging from 50 µm to 1 mm can be attached to the syringe to obtain prints with different resolutions.

2.4. Experimental setup

Various 3D structures composed of three materials were 3D printed using the direct-print system to demonstrate the capability of the developed system. A single taxel sensor was fabricated via the multi-material direct-print system and was subsequently evaluated. The experimental setup to test the sensor consisted of an M5-5 force gauge (Mark-10 Corporation, Copiague, N.Y., USA) with a resolution of 0.005 N, a BNC-2090A data acquisition system (DAQ) from National Instruments (Austin, Texas, USA), an E3630A external power supply (Keysight Technologies, Santa Rosa, Calif., USA), and an A-LSQ075A-E01 motorized linear stage (Zaber Technologies, Vancouver, B.C.,

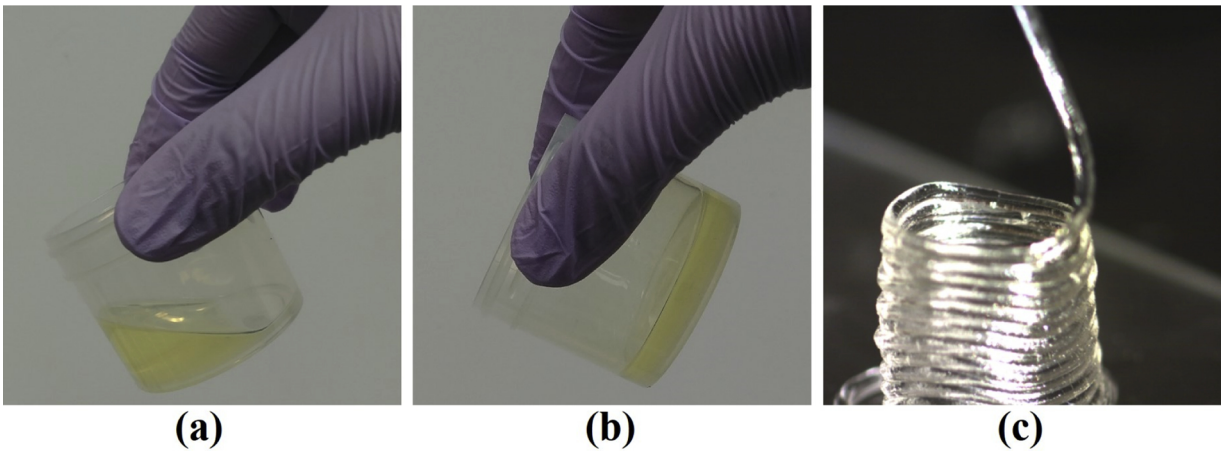

Fig. 2. The photopolymer TangoPlus (*a*) before modification and (*b*) mixed with 10 wt.% fumed silica; (*c*) TangoPlus with 10 wt.% fumed silica when extruded through a printer nozzle.

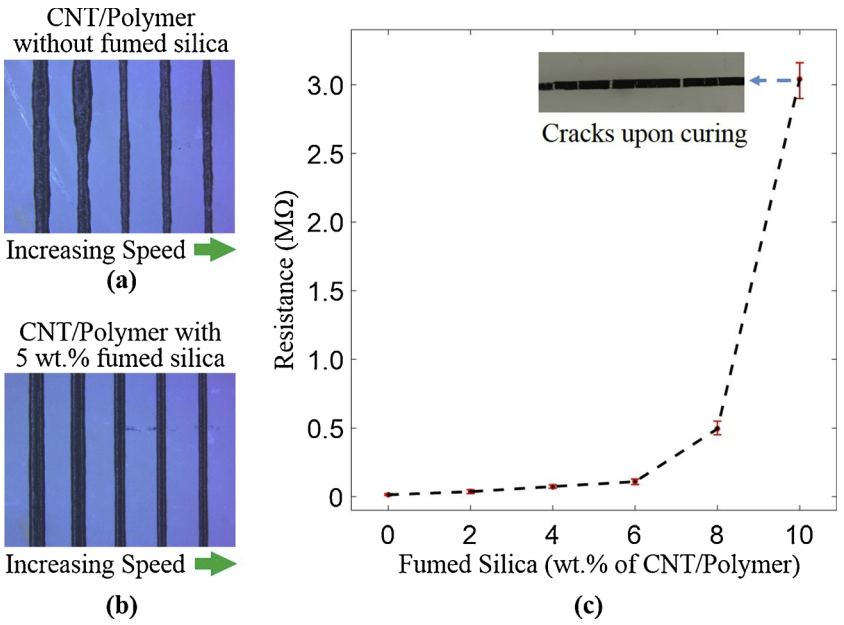

Fig. 3. Lines that were 3D printed using (*a*) CNT/prepolymer material without fumed silica for 7, 10, 15, 18, and 20 mm/s travel speeds for the extruder; and (*b*) CNT/prepolymer material with 5 wt.% fumed silica, printed with similar travel speeds. (*c*) Electrical resistance for CNT/polymer lines vs. wt. % of fumed silica used in the CNT/polymer material.

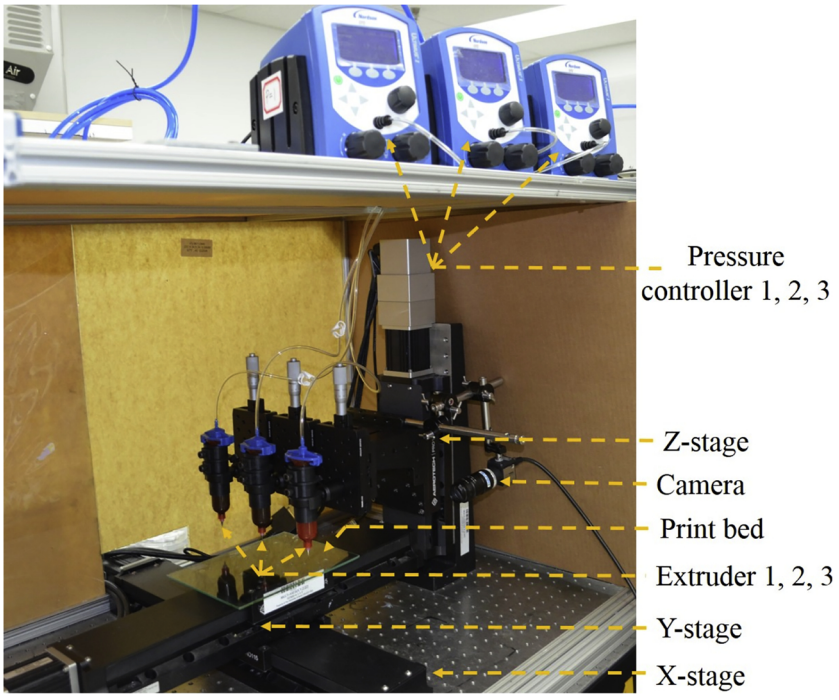

Fig. 4. Multi-material direct-print system.

Canada) having a resolution of 0.1 μm. As shown in Fig. 5(b), the force gauge was attached to the motorized stage and was used to apply compressive force on the taxel. The system was interfaced with MATLAB for collection of sensor data from the DAQ and collection of force data from the force gauge. Fig. 5(a) shows the wiring diagram for the circuit. The sensor was connected to an external resistor (20 MΩ) in series when a 10-V input voltage was supplied through a DC power source. Voltage output across the external resistor was measured as the output signal of the sensor system. The single taxel sensor was examined for different conditions. A 4-taxel (2 × 2) sensor was also fabricated and tested.

3. Results

3.1. Printing of 3D structures

In order to demonstrate the capability of multi-material printing, several 3D structures were printed that involve the use of three extruders in each print. The 3D models were first designed as separate parts for each material in *SolidWorks*. Next, the 3D models were imported into a G-code generator software (*Repetier-Host* and *Slic3r*) to create the tool movement and extrusion instructions for 3D printing. The printing material used for the 3D structures was TangoPlus photopolymer with 10 wt.% fumed silica, and a different color dye was added to the photopolymer for materials loaded into each extruder to distinguish the output from the three extruders. The nozzles/tips used

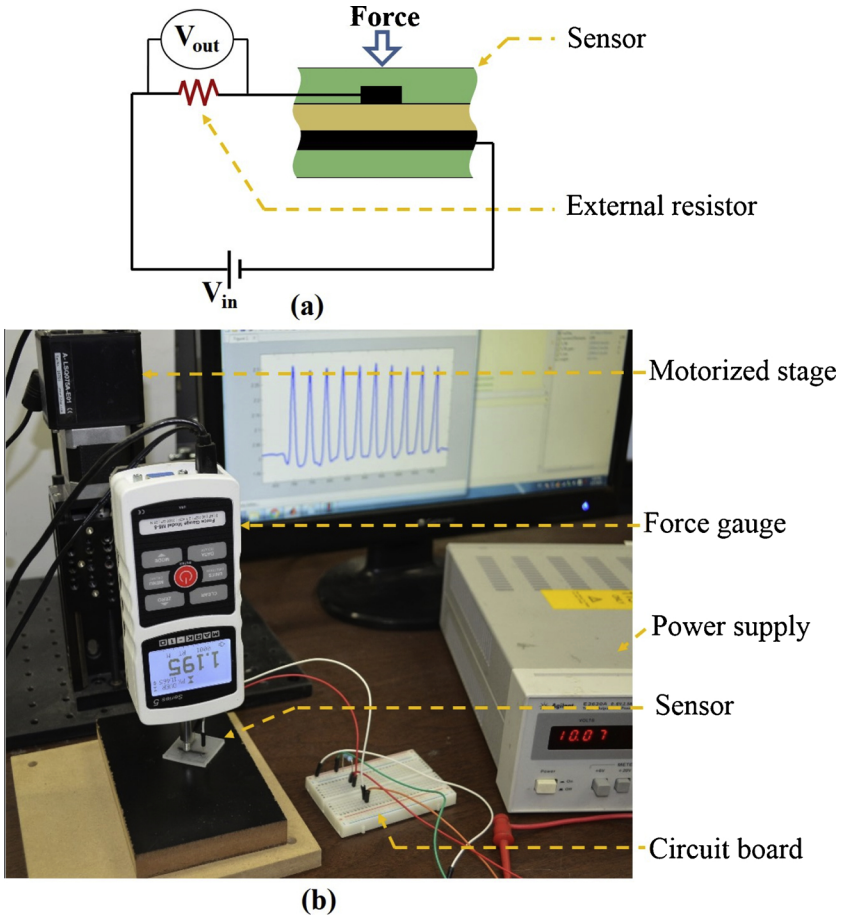

Fig. 5. Sensor evaluation: (*a*) wiring diagram and; (*b*) experimental setup.

for all three extruders had an inner diameter of 335 µm, and the layer height was set at 300 µm with 100% infill for printing. The travel speed was set at 15 mm/s with a dispensing pressure of approximately 16 psi. Fig. 6 shows three 3D parts that were printed with three materials, where each model was built in a single print that involved all three extruders in the printing process.

3.2. Sensor printing

For any 3D printing project, a number of parameters such as nozzle diameter, layer height, travel speed, dispensing pressure, and material composition are involved, and each of these parameters can be varied to adjust the geometry of the printed line. In order to uniformly print a stretchable sensor, the print parameters must be adjusted for each material used in building the sensor to obtain a constant line width throughout the printing process. In this study, an experiment was conducted to determine the appropriate parameters to use for the three printing materials by varying the dispensing pressure while keeping all other parameters fixed. A nozzle/tip with a 335-µm inner diameter was used, the layer height was set at 335 µm, and the travel speed was set at 15 mm/s. Next, lines were printed using different pressures for each material. The line width of the printed lines increased with the increase of pressure, as evident from the images shown in Fig. 7(a). The graph in Fig. 7(b) shows the relationship between line width and pressure for prints made using CNT/prepolymer without fumed silica (FS), CNT/prepolymer with 5 wt.% FS, IL/TangoPlus with 10 wt.% FS, and TangoPlus with 10 wt.% FS. In order to obtain line widths of 335 µm for CNT/prepolymer with FS, IL/TangoPlus with FS, and TangoPlus with FS, the pressures were calculated from the graph to obtain values of 9.1 psi, 15.3 psi, and 16.2 psi, respectively. For the 3D printing process used to print the stretchable sensor, the pressures for the three materials were set around these values so that the linewidths for different materials could be maintained fairly close.

Fig. 8 shows the process for printing the stretchable sensor. Syringes 1, 2, and 3 were loaded with IL/TangoPlus, TangoPlus, and CNT/prepolymer (all modified with FS), respectively. Fig. 8(a) shows bottom layer being printed with TangoPlus using Syringe 2, while Fig. 8(b) and (c) show the intermediate layer and CNT/prepolymer electrode being printed using Syringe 1 and Syringe 3, respectively. A constant tip diameter (335 µm), layer height (335 µm), and travel speed (15 mm/s) were maintained for all three extruders/materials, while the pressure was varied for each material to achieve a constant linewidth. A 30-mm × 30-mm single-taxel sensor was 3D printed with a height of 2.7 mm. The CNT/polymer electrodes were 20 mm × 1.5 mm, which created a 1.5 mm × 1.5 mm taxel. The CNT-based electrodes consist of one print-layer with a height of ~335 µm when the IL-based intermediate layer consists of three print-layers resulting in a height of ~1 mm. Fig. 8(d) shows the 3D printed sensor before curing, fabricated using the multi-material direct-print system. The printed prepolymer part was primarily polymerized using UV light curing system (OmniCure® S2000, Excelitas Technologies Co., Wheeling, IL). As the CNT/prepolymer is partially photocurable because CNTs prohibit the light penetration (i.e., similar effects of using black dyes), the sensor was also maintained at 100 °C for 10 min to cure the CNT-based electrodes thermally. Fig. 8(e) and (f) show the flexible and stretchable sensor after curing. A 4-taxel (2 × 2) sensor was also 3D printed, as will be described in the following section.

3.3. Sensor evaluation

To verify the mechanical characteristics of the stretchable sensor, a

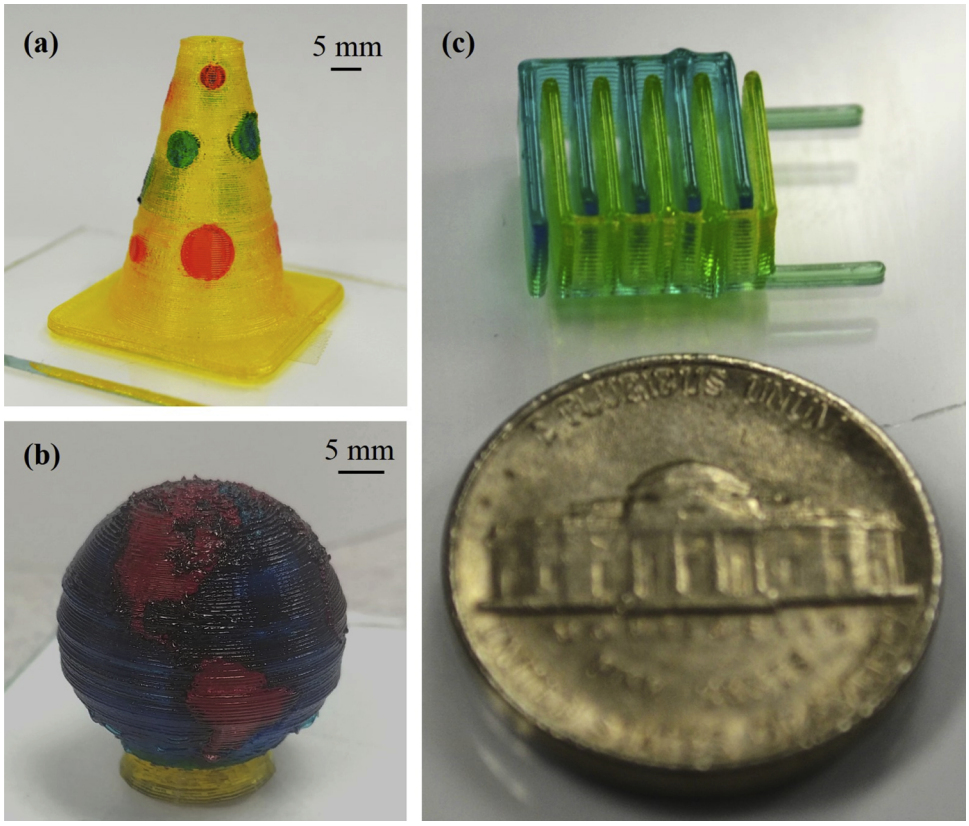

Fig. 6. Examples of 3D structures printed with three materials using the multi-material direct-print system.

dog bone–shaped sensor was 3D printed according to the dimensions given in ASTM D638 for a Type V tensile test specimen, as shown in Fig. 9(a). An Instron 5582 (Instron, Norwood, MA) universal testing machine was used for a tension test and a compression test at a cross-head speeds of 100 mm/min and 1 mm/min, respectively. Fig. 9(b) and (c) show the behavior of the sensor under tension and compression, respectively. Next, the printed single-taxel sensor described in Section 3.2 was evaluated under different compressive forces. A probe having a diameter of 3 mm was attached to the force gauge to apply force on the taxel. First, the sensor was subjected to a fixed strain of 38% for multiple cycles at a probe speed of 0.5 mm/s. Fig. 10(a) shows the applied force and the change in voltage output (ΔV_{out}) of the sensor system that

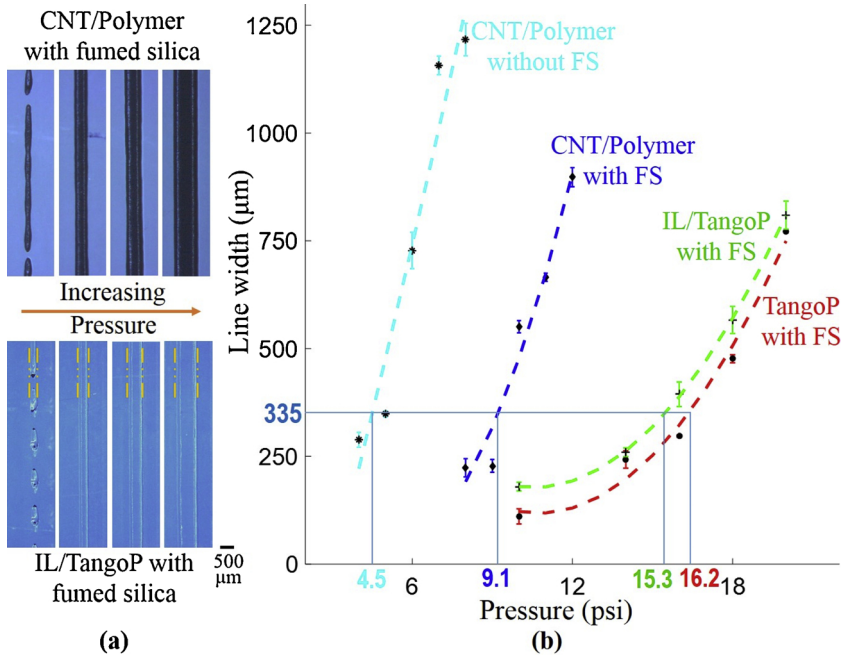

Fig. 7. (*a*) Microscope image of lines printed with CNT/prepolymer with fumed silica (FS) and those printed with IL/TangoPlus with FS for increasing pressure; (*b*) line width vs. pressure for different materials, where all other printing parameters were fixed.

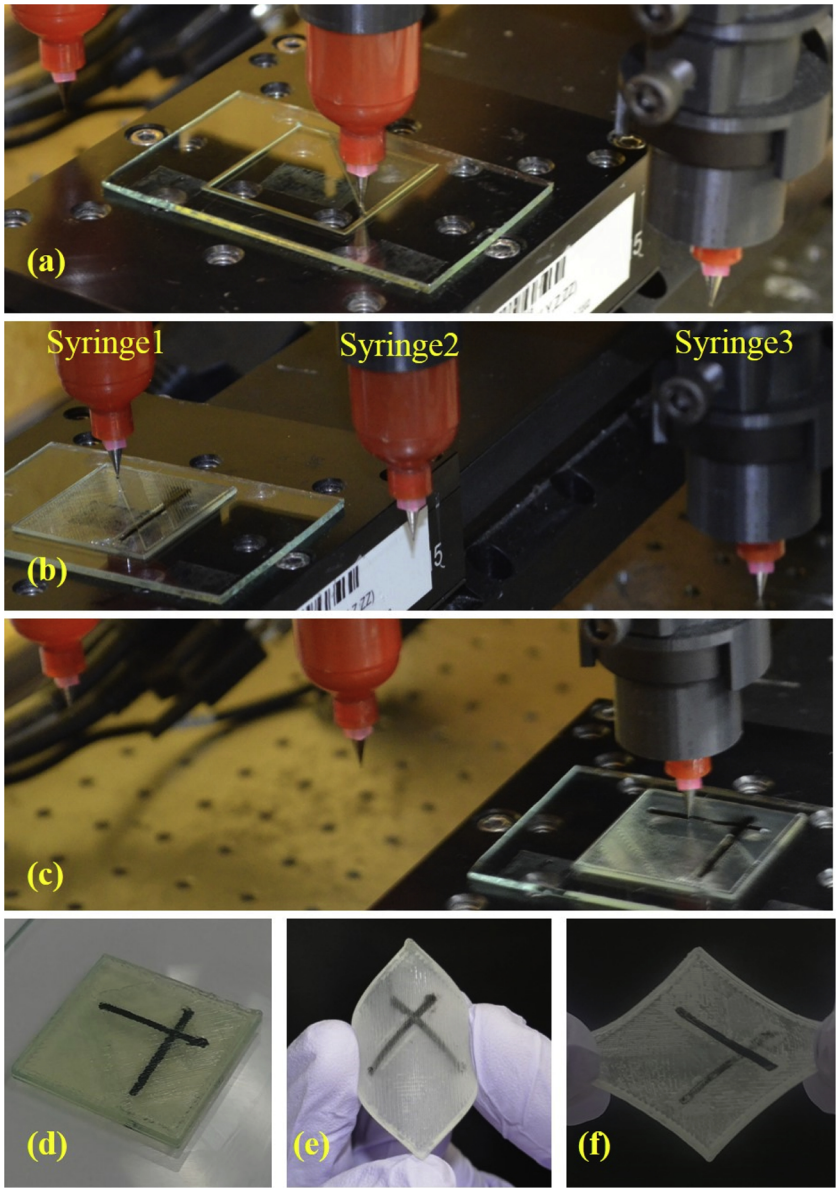

Fig. 8. Multi-material direct-print process for a single-taxel sensor: (*a*) bottom layer printed using modified TangoPlus; (*b*) intermediate layer printed using modified IL/TangoPlus; (*c*) Conductive electrode printing using modified CNT/prepolymer; (*d*) printed sensor before curing; (*e–f*) Cured flexible and stretchable sensor.

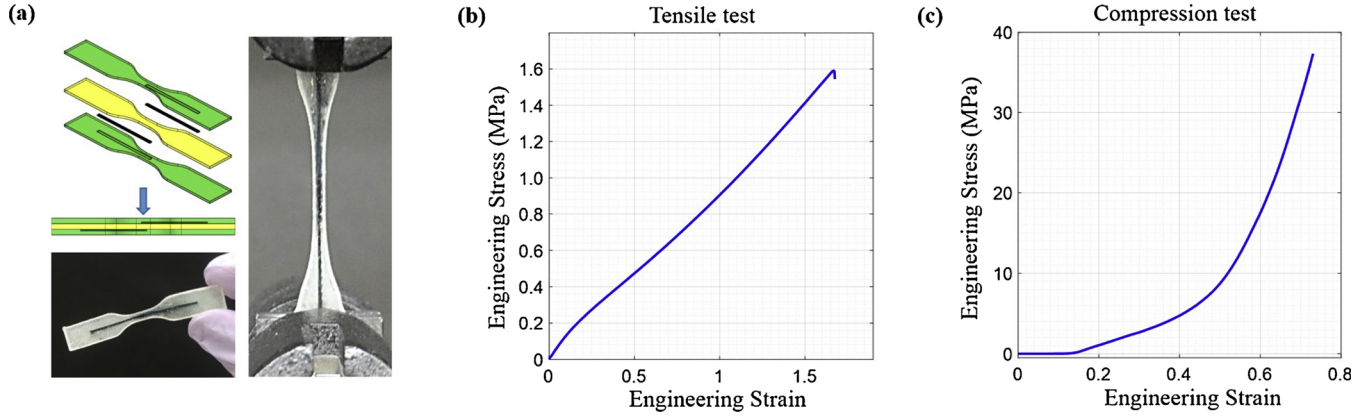

Fig. 9. Mechanical characteristics of the sensor: (*a*) Dog-bone shaped 3D printed sensor specimen used for tensile test; (*b*) tensile test of the printed sensor; (*c*) compression test with the printed sensor.

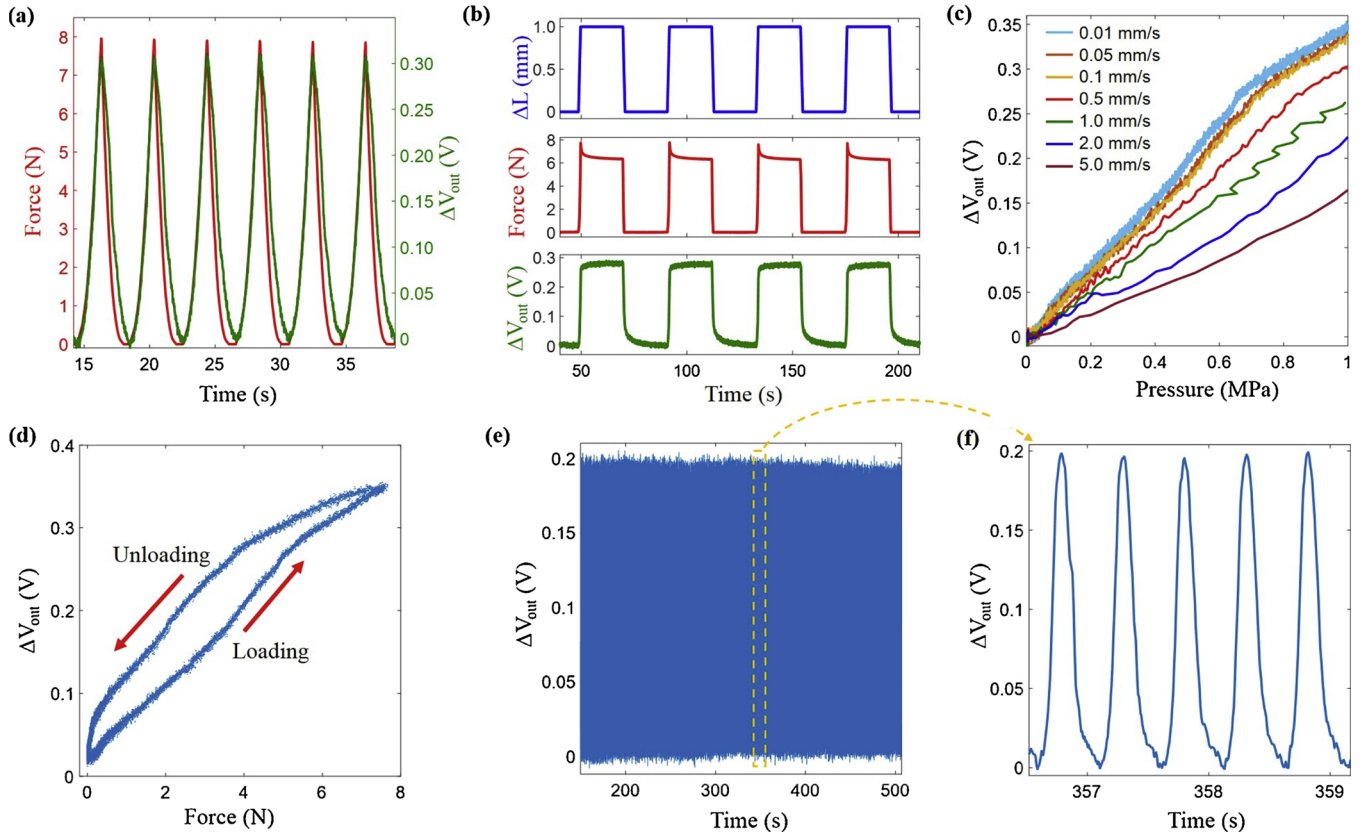

Fig. 10. Sensor evaluation: (*a*) applied force and sensor output (ΔV_{out}) for a fixed strain loop; (*b*) probe displacement (ΔL) from the point of contact (in blue), force (in red), and ΔV_{out} (in green) at the same timestamp; (c) ΔV_{out} vs. pressure for different probe speeds, showing the strain rate dependence; and (*d*) hysteresis curve for 10 loops. (e) Sensor subjected to 1000 pressing cycles of a constant strain and (*f*) a subset of (*e*) that shows several cycles with a consistent output. (For interpretation of the references to colour in this figure legend, the reader is referred to the web version of this article).

were recorded at the same timestamp. As can be noticed from this figure, while the loading curves for force and ΔV_{out} are similar, a difference in the unloading curve can be observed. This difference in unloading may occur due to the viscoelastic properties of the soft sensor, which will be discussed in the following section. Also, time delay between the applied force and ΔV_{out} is less than ten milliseconds.

Fig. 10(b) shows the result from an additional experiment, where a strain at a certain level was maintained on the sensor over a period of time. In the top graph of Fig. 10(b), ΔL indicates the probe/stage displacement from the point of contact with the sensor. This figure shows multiple loops where a 1-mm probe displacement was applied on the sensor for 20 s, and the applied force and ΔV_{out} are also shown for the same timestamp. The force does not remain constant over time because of the stress relaxation in the viscoelastic TangoPlus elastomer, where the sensor output ΔV_{out} is driven by the strain in the sensor.

The strain rate/deformation rate–dependence of the sensor response is shown in Fig. 10(c). Compressive forces were applied on the sensor at different probe speeds, and ΔV_{out} vs. pressure curves were constructed. The viscoelastic polymers show strain rate–dependent stress–strain characteristics [51]. For the same stress, a lower deformation rate requires a higher strain. As a result, a lower probe speed results in a higher ΔV_{out}, as illustrated in Fig. 10(c). The difference between loading and unloading behavior can be seen in in Fig. 10(d), which presents a hysteresis curve for 10 loops. A 35% strain was applied on the sensor at a probe speed of 0.1 mm/s. The sensor also exhibited consistent responses when it was subjected to more than 1000 pressing cycles. Fig. 10(e) shows a segment of the sensor response when the sensor was under a 38% strain cycle at a probe speed of 5 mm/s for more than 1000 cycles. Fig. 10(f) shows a portion of the response in Fig. 10(e) and illustrates the consistency of the sensor output over time.

When there is a need for pressure profiling of a larger area and/or a need to locate the point of pressure application, a multi-taxel sensor could be employed, and the configuration of the electrode arrays in the sensor could be customized in order to generate a different number and density of taxels. To verify that the proposed sensor could also be 3D printed with multiple taxels, a 4-taxel (2 × 2) sensor was 3D printed via the multi-material direct-print system, as shown in Fig. 11(a). The sensor was connected to external circuitry so that data could be collected from all four taxels simultaneously. Force was applied manually on one taxel, as shown in Fig. 11(b), and the resulting sensor response in all the taxels in terms of ΔV_{out} is shown in Fig. 11(c). The taxel that underwent deformation showed a peak in ΔV_{out} at the time of force application.

4. Discussion

The printing parameters for three different materials in the sensor were investigated for using in the multi-material direct-print system developed in this study, and the system was successfully implemented in the fabrication of a soft stretchable sensor as well as other multi-material structures. While the soft sensor fabricated in this study showed consistent performance throughout the evaluation process, there are still some opportunities for improvement of the proposed printing system. For example, a wiper brush and the corresponding motion instructions could be added to the system to enable cleaning of the extruder nozzle after each layer, as this would prevent contamination between materials. A brush could be placed near the print-bed and G-code commands could be added to have few back-and-forth movements of the nozzle on the brush. Currently, tips are manually wiped, if needed. Also, the modification of the IL/polymer and CNT/

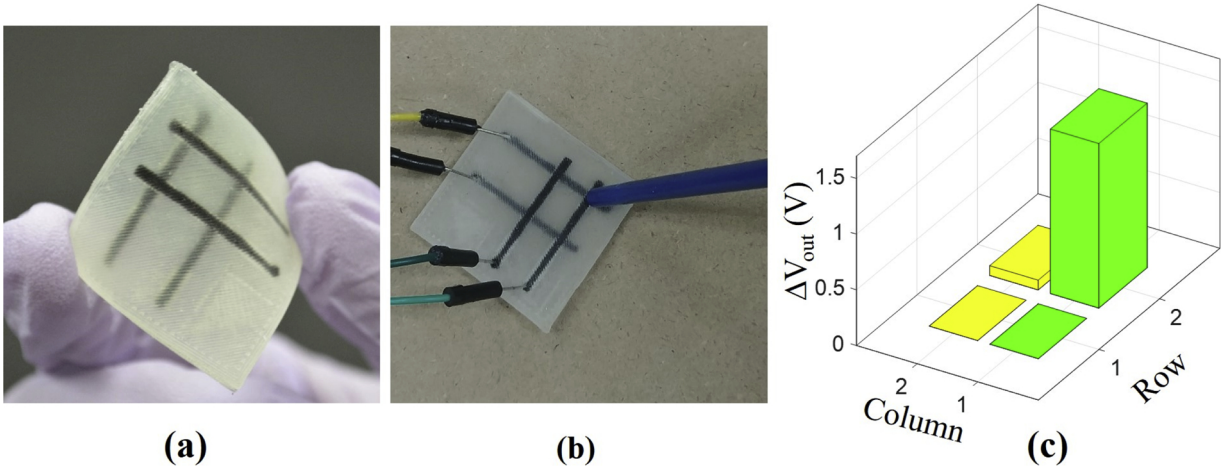

Fig. 11. The 4-taxel sensor: (a) Finished sensor that was 3D printed using the direct-print system. (b) Pressure applied on one of the taxels; and (c) output data showing ΔV_{out} on that taxel.

polymer composite with fumed silica could have some adverse effect on sensing performance and mechanical pliability. However, as evident in Section 3.2, the printed sensor showed reliable sensitivity to external strain which is the target property in the sensor. It is possible to calibrate the printed sensor according to its response. In addition, the sensor geometry and material composition can be easily varied to fine-tune the sensing performance.

The unloading behavior is different from the loading behavior for the stretchable sensor, as can be noticed from Fig. 10(a) and (d). The hysteresis error for a probe speed of 0.1 mm/s was calculated to be approximately 30%. This is a common phenomenon for viscoelastic elastomers due to their time-dependent elastic properties [52,53]. However, there is consistency in the loading and unloading curves over multiple cycles. Fig. 10(d) shows the results for 10 cycles where all the loading curves are similar and all unloading curves are similar but follow a different path. Thus, the sensor is able to provide a predictable response. Fig. 10(b) shows stress relaxation under a constant strain, where part of the deformational energy is stored elastically and part of it is dissipated through viscous mechanisms [52]. This ability of the sensor to dissipate energy could be useful when there is a need for shock absorption, such as for smart insoles [12] and smart helmets [54]. The sensor also shows a deformation rate/strain rate–dependent response, as shown in Fig. 10(c). The viscoelastic materials cannot rearrange their molecules quickly enough during a short excitation to accommodate to the strain. In contrast, during a long excitation, there is sufficient time for molecular rearrangement to occur [52], which is why the sensors show deformation rate–dependent behavior. Overall, the sensor showed a reliable and consistent response over a few thousand pressing cycles.

5. Conclusions

In this work, a multi-material direct-print system was developed that is capable of printing functional materials. An IL-based soft pressure sensor was 3D printed using the developed system. Materials were modified for 3D printing but were able to maintain their functionality. Introducing IL in the fabrication of a soft pressure sensor gives more control over sensor performance, and this opens new possibilities for research and application. Multi-material 3D printing can provide unparalleled manufacturing and design flexibility, as it enables the use of a wide variety of materials. The flexibility and stretchability of the developed soft sensor make it suitable for applications where parts are moveable or are subjected to bending, flexing, and impact, as the 3D printing process enables sensors to be fabricated on a freeform surface with a complex geometry. Future studies will focus on upgrading the direct-print system, investigating conformal 3D printing of stretchable sensors, and further optimizing the materials used for printing. The work presented in this study is believed to enhance the research on 3D printed soft electronics and to open new avenues in the area of wearable devices, smart technologies, human-machine interfaces, and prosthetics.

Conflict of interest

None.

Acknowledgements

This work was supported by research grants from Center for Tire Research (CenTiRe, Subaward #445530-19D17B under NSF prime award #IIP-1650423) and Faculty Research Committee of The University of Akron. It is noted that Dr. Alkadi recieved a full scholarship incompleting this work supported by Jazan University through Saudi Arabian Cultural Mission (SCAM). It is also noted that Dr. Alkadi and Mr. Emon are co-first authors with an equal contribution in this work.

References

[1] Z. Bao, X. Chen, Flexible and stretchable devices, Adv. Mater. 28 (2016) 4177–4179, https://doi.org/10.1002/adma.201601422.
[2] D.P. Dubal, N.R. Chodankar, D.-H. Kim, P. Gomez-Romero, Towards flexible solid-state supercapacitors for smart and wearable electronics, Chem. Soc. Rev. 47 (2018) 2065–2129, https://doi.org/10.1039/C7CS00505A.
[3] S. Bauer, S. Bauer-Gogonea, I. Graz, M. Kaltenbrunner, C. Keplinger, R. Schwödiauer, 25th anniversary article: a soft future: from robots and sensor skin to energy harvesters, Adv. Mater. 26 (2014) 149–162, https://doi.org/10.1002/adma.201303349.
[4] N. Lu, D.-H. Kim, Flexible and stretchable electronics paving the way for soft robotics, Soft Robot. 1 (2013) 53–62, https://doi.org/10.1089/soro.2013.0005.
[5] A. Chortos, J. Liu, Z. Bao, Pursuing prosthetic electronic skin, Nat. Mater. 15 (2016) 937–950, https://doi.org/10.1038/nmat4671.
[6] S. Kumbay Yildiz, R. Mutlu, G. Alici, Fabrication and characterisation of highly stretchable elastomeric strain sensors for prosthetic hand applications, Sens. Actuators A: Phys. 247 (2016) 514–521, https://doi.org/10.1016/j.sna.2016.06.037.
[7] M. Amjadi, K.-U. Kyung, I. Park, M. Sitti, Stretchable, skin-mountable, and wearable strain sensors and their potential applications: a review, Adv. Funct. Mater. 26 (2016) 1678–1698, https://doi.org/10.1002/adfm.201504755.
[8] X. Wang, Z. Liu, T. Zhang, Flexible sensing electronics for wearable/attachable health monitoring, Small 13 (2017) 1602790, , https://doi.org/10.1002/smll.201602790.
[9] C. Dagdeviren, P. Joe, O.L. Tuzman, K.-I. Park, K.J. Lee, Y. Shi, Y. Huang, J.A. Rogers, Recent progress in flexible and stretchable piezoelectric devices for mechanical energy harvesting, sensing and actuation, Extrem. Mech. Lett. 9 (2016) 269–281, https://doi.org/10.1016/j.eml.2016.05.015.
[10] X. Wang, T. Xu, S. Dong, S. Li, L. Yu, W. Guo, H. Jin, J. Luo, Z. Wu, J. Min King, Development of a flexible and stretchable tactile sensor array with two different

structures for robotic hand application, RSC Adv. 7 (2017) 48461–48465, https://doi.org/10.1039/C7RA08605A.
[11] A.P. Gerratt, H.O. Michaud, S.P. Lacour, Elastomeric electronic skin for prosthetic tactile sensation, Adv. Funct. Mater. 25 (2015) 2287–2295, https://doi.org/10.1002/adfm.201404365.
[12] M.O.F. Emon, J.-W. Choi, A preliminary study on 3D printed smart insoles with stretchable piezoresistive sensors for plantar pressure monitoring, ASME 2017 International Mechanical Engineering Congress and Exposition (2017), https://doi.org/10.1115/IMECE2017-71817 p. V002T02A028-V002T02A028.
[13] T.Q. Trung, N.-E. Lee, Flexible and stretchable physical sensor integrated platforms for wearable human-activity monitoring and personal healthcare, Adv. Mater. 28 (2016) 4338–4372, https://doi.org/10.1002/adma.201504244.
[14] X. Chen, C. Zhang, C. Ma, H. Liu, Y. Zheng, Y. Jiang, Y. Zu, J. Niu, Evaluation of helmet comfort based on flexible pressure sensor matrix, in: W. Karwowski, T. Ahram (Eds.), Intelligent Human Systems Integration 2019, Springer International Publishing, 2019, pp. 833–839, , https://doi.org/10.1007/978-3-030-11051-2_127 HTTPS://.
[15] Y. Li, S. Luo, M.-C. Yang, R. Liang, C. Zeng, Poisson ratio and piezoresistive sensing: a new route to high-performance 3D flexible and stretchable sensors of multimodal sensing capability, Adv. Funct. Mater. 26 (2016) 2900–2908, https://doi.org/10.1002/adfm.201505070.
[16] F. Khatyr, C. Imberdis, P. Vescovo, D. Varchon, J.-M. Lagarde, Model of the viscoelastic behaviour of skin in vivo and study of anisotropy, Skin Res. Technol. 10 (2004) 96–103, https://doi.org/10.1111/j.1600-0846.2004.00057.x.
[17] M.O.F. Emon, J.-W. Choi, Flexible piezoresistive sensors embedded in 3D printed tires, Sensors 17 (2017) 656, https://doi.org/10.3390/s17030656.
[18] Y.-S. Hong, Smart Care Beds for Elderly Patients with Impaired Mobility, Wirel. Commun. and Mob. Comput., 2018, https://doi.org/10.1155/2018/1780904.
[19] D. Hera, A. Berndt, T. Günther, S. Schmiel, C. Harendt, A. Zimmermann, Flexible packaging by film-assisted molding for microintegration of inertia sensors, Sensors 17 (2017) 1511, https://doi.org/10.3390/s17071511.
[20] I. Teyeb, O. Jemai, M. Zaied, C.B. Amar, Towards a Smart Car Seat Design for Drowsiness Detection Based on Pressure Distribution of the Driver's Body, ICSEA, 2016, p. 230 2016.
[21] M.K. Yapici, T.E. Alkhidir, Intelligent medical garments with graphene-functionalized smart-cloth ECG sensors, Sensors 17 (2017) 875, https://doi.org/10.3390/s17040875.
[22] M. Amjadi, Y.J. Yoon, I. Park, Ultra-stretchable and skin-mountable strain sensors using carbon nanotubes–ecoflex nanocomposites, Nanotechnol. 26 (2015) 375501, , https://doi.org/10.1088/0957-4484/26/37/375501.
[23] M. Vatani, E.D. Engeberg, J.-W. Choi, Force and slip detection with direct-write compliant tactile sensors using multi-walled carbon nanotube/polymer composites, Sens. Actuators A Phys. 195 (2013) 90–97, https://doi.org/10.1016/j.sna.2013.03.019.
[24] H. Hocheng, C.-M. Chen, Design, fabrication and failure analysis of stretchable electrical routings, Sensors 14 (2014) 11855–11877, https://doi.org/10.3390/s140711855.
[25] N. Alamusi, H. Hu, S. Fukunaga, Y. Atobe, J. Li Liu, Piezoresistive strain sensors made from carbon nanotubes based polymer nanocomposites, Sensors 11 (2011) 10691–10723, https://doi.org/10.3390/s111110691.
[26] M. Vatani, M. Vatani, J.W. Choi, Multi-layer stretchable pressure sensors using ionic liquids and carbon nanotubes, Appl. Phys. Lett. 108 (2016) 061908, , https://doi.org/10.1063/1.4941812.
[27] D.Y. Choi, M.H. Kim, Y.S. Oh, S.-H. Jung, J.H. Jung, H.J. Sung, H.W. Lee, H.M. Lee, Highly stretchable, hysteresis-free ionic liquid-based strain sensor for precise human motion monitoring, ACS Appl. Mater. Interfaces 9 (2017) 1770–1780, https://doi.org/10.1021/acsami.6b12415.
[28] K.N. Marsh, J.A. Boxall, R. Lichtenthaler, Room temperature ionic liquids and their mixtures—a review, Fluid Phase Equilib. 219 (2004) 93–98, https://doi.org/10.1016/j.fluid.2004.02.003.
[29] H. Ohno, Design of ion conductive polymers based on ionic liquids, Macromol. Symp. 249–250 (2007) 551–556, https://doi.org/10.1002/masy.200750435.
[30] H. Ota, K. Chen, Y. Lin, D. Kiriya, H. Shiraki, Z. Yu, T.-J. Ha, A. Javey, Highly deformable liquid-state heterojunction sensors, Nat. Commun. 5 (2014) 5032, https://doi.org/10.1038/ncomms6032.
[31] J.-B. Chossat, H.-S. Shin, Y.-L. Park, V. Duchaine, Soft tactile skin using an embedded ionic liquid and tomographic imaging, J. Mech. Rob. 7 (2015), https://doi.org/10.1115/1.4029474 021008-021008–9.
[32] J. Chossat, Y. Park, R.J. Wood, V. Duchaine, A soft strain sensor based on ionic and metal liquids, IEEE Sens. J. 13 (2013) 3405–3414, https://doi.org/10.1109/JSEN.2013.2263797.
[33] J. Lee, M.O.F. Emon, M. Vatani, J.-W. Choi, Effect of degree of crosslinking and polymerization of 3D printable polymer/ionic liquid composites on performance of stretchable piezoresistive sensors, Smart Mater. Struct. 26 (2017) 035043, , https://doi.org/10.1088/1361-665X/aa5c70.
[34] D.M. Vogt, Y. Park, R.J. Wood, Design and characterization of a soft multi-axis force sensor using embedded microfluidic channels, IEEE Sens. J. 13 (2013) 4056–4064, https://doi.org/10.1109/JSEN.2013.2272320.
[35] W. Hu, X. Niu, R. Zhao, Q. Pei, Elastomeric transparent capacitive sensors based on an interpenetrating composite of silver nanowires and polyurethane, Appl. Phys. Lett. 102 (2013) 083303, , https://doi.org/10.1063/1.4794143.
[36] C. Majidi, R. Kramer, R.J. Wood, A non-differential elastomer curvature sensor for softer-than-skin electronics, Smart Mater. Struct. 20 (2011) 105017, , https://doi.org/10.1088/0964-1726/20/10/105017.
[37] C. Lee, L. Jug, E. Meng, High strain biocompatible polydimethylsiloxane-based conductive graphene and multiwalled carbon nanotube nanocomposite strain sensors, Appl. Phys. Lett. 102 (2013) 183511, , https://doi.org/10.1063/1.4804580.
[38] T.D. Ngo, A. Kashani, G. Imbalzano, K.T.Q. Nguyen, D. Hui, Additive manufacturing (3D printing): a review of materials, methods, applications and challenges, Compos. Part B: Eng. 143 (2018) 172–196, https://doi.org/10.1016/j.compositesb.2018.02.012.
[39] L.E. Murr, Frontiers of 3D printing/additive manufacturing: from human organs to aircraft fabrication†, J. Mater. Sci. Technol. 32 (2016) 987–995, https://doi.org/10.1016/j.jmst.2016.08.011.
[40] S.-Z. Guo, K. Qiu, F. Meng, S.H. Park, M.C. McAlpine, 3D printed stretchable tactile sensors, Adv. Mater. 29 (2017) 1701218, , https://doi.org/10.1002/adma.201701218.
[41] Z. Weng, J. Wang, T. Senthil, L. Wu, Mechanical and thermal properties of ABS/montmorillonite nanocomposites for fused deposition modeling 3D printing, Mater. Des. 102 (2016) 276–283, https://doi.org/10.1016/j.matdes.2016.04.045.
[42] J. Lee, Y. Lu, S. Kashyap, A. Alarmdari, M.O.F. Emon, J.-W. Choi, Liquid bridge microstereolithography, Addit. Manuf. 21 (2018) 76–83, https://doi.org/10.1016/j.addma.2018.02.012.
[43] S. Meteyer, X. Xu, N. Perry, Y.F. Zhao, Energy and material flow analysis of binder-jetting additive manufacturing processes, Procedia Cirp 15 (2014) 19–25, https://doi.org/10.1016/j.procir.2014.06.030.
[44] S.F.S. Shirazi, S. Gharehkhani, M. Mehrali, H. Yarmand, H.S.C. Metselaar, N.A. Kadri, N.A.A. Osman, A review on powder-based additive manufacturing for tissue engineering: selective laser sintering and inkjet 3D printing, Sci. Technol. Adv. Mater. 16 (2015) 033502, , https://doi.org/10.1088/1468-6996/16/3/033502.
[45] T.A. Campbell, O.S. Ivanova, 3D printing of multifunctional nanocomposites, Nano Today 8 (2013) 119–120, https://doi.org/10.1016/j.nantod.2012.12.002.
[46] M. Vatani, E.D. Engeberg, J.-W. Choi, Conformal direct-print of piezoresistive polymer/nanocomposites for compliant multi-layer tactile sensors, Addit. Manuf. 7 (2015) 73–82, https://doi.org/10.1016/j.addma.2014.12.009.
[47] X. Wang, M. Jiang, Z. Zhou, J. Gou, D. Hui, 3D printing of polymer matrix composites: a review and prospective, Compos. Part B: Eng. 110 (2017) 442–458, https://doi.org/10.1016/j.compositesb.2016.11.034.
[48] N. Grossiord, J. Loos, L. van Laake, M. Maugey, C. Zakri, C.E. Koning, A.J. Hart, High-conductivity polymer nanocomposites obtained by tailoring the characteristics of carbon nanotube fillers, Adv. Funct. Mater. 18 (2008) 3226–3234, https://doi.org/10.1002/adfm.200800528.
[49] M. Vatani, J.-W. Choi, Direct-print photopolymerization for 3D printing, Rapid Prototyp. J. 23 (2017) 337–343, https://doi.org/10.1108/RPJ-11-2015-0172.
[50] M.O.F. Emon, J. Lee, U.H. Choi, D. Kim, K. Lee, J. Choi, Characterization of a soft pressure sensor on the basis of ionic liquid concentration and thickness of the piezoresistive layer, IEEE Sens. J. (2019), https://doi.org/10.1109/JSEN.2019.2911859 In Press.
[51] V. Slesarenko, S. Rudykh, Towards mechanical characterization of soft digital materials for multimaterial 3D-printing, Int. J. Eng. Sci. 123 (2018) 62–72, https://doi.org/10.1016/j.ijengsci.2017.11.011.
[52] N.W. Tschoegl, Time dependence in material properties: an overview, Mech. of Time-Depend. Mater. 1 (1997) 3–31, https://doi.org/10.1023/A:1009748023394.
[53] L. Qiu, M.B. Coskun, Y. Tang, J.Z. Liu, T. Alan, J. Ding, V.-T. Truong, D. Li, Ultrafast dynamic piezoresistive response of graphene-based cellular elastomers, Adv. Mater. 28 (2016) 194–200, https://doi.org/10.1002/adma.201503957.
[54] W.V. Rosenberg, T. Chanwimalueang, V. Goverdovsky, D. Looney, D. Sharp, D.P. Mandic, Smart helmet: wearable multichannel ECG and EEG, IEEE J. Transl. Eng. Health Med. 4 (2016) 1–11, https://doi.org/10.1109/JTEHM.2016.2609927.